Articles

Surface Studies of Potentially Protective Films on Gadolinium

Sajan Thomas and Peter M. A. Sherwood*

Department of Chemistry, Willard Hall, Kansas State University, Manhattan, Kansas 66506

Kwan-Myung Lee and Michael J. O'Shea

Department of Physics, Cardwell Hall, Kansas State University, Manhattan, Kansas 66506

Received June 23, 1989

X-ray photoelectron spectroscopy combined with argon-ion depth profiling, Rutherford backscattering, and X-ray diffraction has been used to monitor the surface chemistry of bilayer thin films consisting of an approximately 2000-Å-thick gadolinium layer on an aluminum substrate covered with an evaporated layer of silicon/aluminum, titanium, or aluminum. The latter two films were laser annealed. The silicon/aluminum layer showed both silicon and a possible aluminosilicate. The outer aluminum layer of the laser-annealed aluminum film showed both metal and oxide, but much less metal than expected for an evaporated film. Laser annealing provides a gently graded interface between the outer layer and the inner gadolinium layer. There was evidence for mixing of the aluminum and gadolinium layers and the formation of gadolinium–aluminum oxides. The gadolinium layer was oxidized, especially in the case of the titanium outer layer. The greatest protection from oxidation was provided by the aluminum-containing outer layers.

Introduction

The rare earth (RE) and rare earth–transition metal (RE–TM) alloys are an important class of materials technologically with important applications associated with their magnetic properties, including thin-film erasable recording media[1,2] and permanent magnets both thin film[3,4] and bulk.[5,6] The high affinity of the rare earths for oxygen presents problems in the preparation and application of rare-earth-containing materials. Oxidation is the principal form of "aging" in such materials. Evidence for this comes from the many studies on RE–TM alloys where, for example, the magnetization, coercivity, and Faraday or Kerr rotation angle change with time as the alloy is oxidized.

Attempts have been made to prevent oxidation of the RE–TM magnetic media by using protective oxide films[7-9] and metal coatings.[10] The purpose of this work is to study the surface and near-surface chemistry of a rare earth film covered with different potentially protective surface layers. In this study we have coated gadolinium thin films with a nonmagnetic protective film involving titanium, silicon, and/or aluminum. These materials were chosen as the protective layers since they are known to form stable and mechanically hard oxides. We modified the surface-protective layer by laser annealing the surface of two of the layers (titanium and aluminum) and coevaporating (silicon/aluminum) a surface layer in the third case. Both laser annealing and coevaporation have the potential to modify the surface layer by forming surface alloys and, in the case of laser annealing, causing surface mixing. We report the surface chemistry of these layers, and in the case of one of the layers (titanium) we report the change in surface chemistry over a range of temperatures.

Experimental Section

The thin films were prepared by using an ion-pumped evaporation system operating at 5×10^{-8} Torr. Films were evaporated onto an aluminum substrate. First an approximately 2000–4000-Å-thick gadolinium (using a 99.95% purity sample) film was evaporated onto the substrate, and then the outer protective film. The aim was to obtain approximately equal thickness outer layers, though after the evaporation process we estimated (from weight loss measurements) that there were approximately 100 Å of titanium, 200 Å of coevaporated aluminum and silicon, and 140 Å of aluminum evaporated in the three cases studied. The aluminum, silicon, and titanium samples used in these studies were 99.99% pure. The samples with titanium and with aluminum protective films were laser annealed over a 1-cm^2 area by using a pulsed excimer laser in air. The sample was scanned in the beam by using an $X-Y$ scanning stage. The laser beam at the sample was 0.2 mm in diameter, and an energy of 0.05 J/cm^2 was used. This energy is half of the threshold energy for visible damage to the sample to occur.

Rutherford backscattering spectra were obtained by using the tandem van de Graaff accelerator in the Macdonald Laboratory at Kansas State University. Two different projectiles were used, carbon and lithium at 3 MeV. The lighter projectile was used to obtain more surface-sensitive information. The heavier carbon projectile gives more depth information.

X-ray powder diffraction studies were carried out by using a Scintag $\theta-\theta$ instrument using Cu X-rays. Two geometries were used, a standard geometry ($\theta-\theta$) where the source and detector are scanned together and a surface-sensitive geometry in which the X-rays are incident at 5° to the surface and the detector scanned.

The X-ray photoelectron (XPS or ESCA) spectra were collected on a VSW HA100 X-ray photoelectron spectrometer with a base pressure of in the 10^{-10}-Torr pressure range. The XPS spec-

(1) Kryder, M. H. *J. Appl. Phys.* **1985**, *57*, 3913.
(2) Hong, M.; Bacon, D. D.; Nakahara, S. *J. Appl. Phys.* **1987**, *61*, 3329.
(3) Cadieu, F. J. *J. Appl. Phys.* **1987**, *61*, 4105.
(4) Stancil, D. D. *J. Appl. Phys.* **1987**, *61*, 4111.
(5) See, for example, Nd–Fe–B panel discussion: *IEEE Trans. Magn.* **1986**, *MAG-22*, 904.
(6) Permanent Magnet Workshop, *J. Appl. Phys.* **1987**, *57*, 4081.
(7) Luborsky, F. E. *IEEE Trans. Magn.* **1986**, *MAG-22*, 937.
(8) Hatwar, T. K.; Shin, S. C.; Stinson, D. G. *IEEE Trans. Magn.* **1986**, *MAG-22*, 946.
(9) Miyazaki, M.; Shibata, I.; Okada, S.; Ito, K.; Ogawa, S. *J. Appl. Phys.* **1987**, *61*, 3326.
(10) Hartmann, M.; Witter, K.; Reck, J.; Tolle, H. J. *IEEE Trans. Magn.* **1986**, *MAG-22*, 943.

0897-4756/90/2802-0007$02.50/0

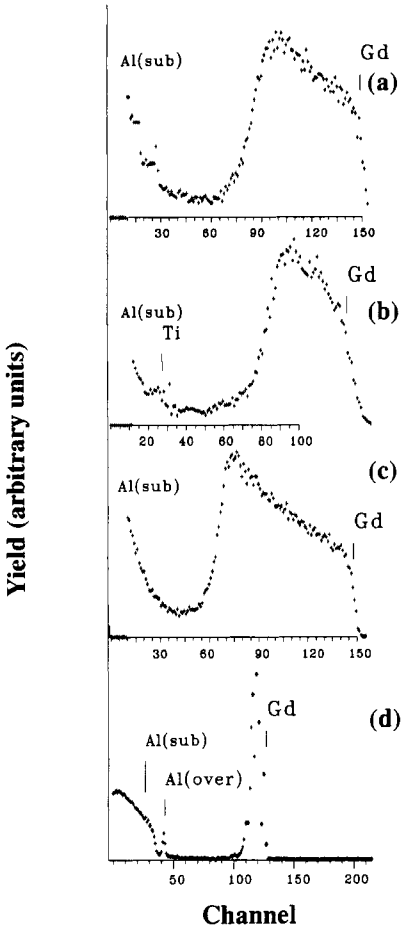

Figure 1. Rutherford backscattering spectra of the films: (a, d) aluminum laser annealed outer film; (b) titanium laser annealed outer film; (c) aluminum/silicon coevaporated outer film; (a–c) 3-MeV carbon projectiles are used; (d) 3-MeV lithium projectiles are used.

trometer was operated in the constant pass energy (FAT) mode (pass energy 10 eV) using Al $K_{\alpha_{1,2}}$ X-ray radiation (300 W). Analyzer resolution was of the same order as the X-ray line width (0.9 eV). Typical data collection times were C 1s (1 h), O 1s (2 h), A 2p (2 h), Si 2p (2 h), Ti 2p (2 h), and Gd 4d (4 h). No sample decomposition was observed during data collection. The spectrometer energy scale was calibrated by using copper and silver[11] and using the separation (233 eV) between photoelectron peaks generated by Mg and Al $K_{\alpha_{1,2}}$ X-rays. Data collection contained a minimum of 33 points per electronvolt. Spectra were recorded immediately after film disposition, and samples were transferred in an inert environment, though some surface oxidation may have occurred during transfer.

The curve fitting of the XPS spectra was carried out by using a nonlinear least-squares curve-fitting program with a Gaussian/Lorentzian product function.[12,13] The Gaussian/Lorentzian mix was taken as 0.5, except for the "graphitic" carbon peak, which was taken as 0.84 with an exponential tail. The C 1s binding energy of residual carbon was taken as 284.6 eV for calibration purposes.

Results and Discussion

Thin-Film Composition. Rutherford backscattering studies of the three films are shown in Figure 1 (E_B (abscissa) refers to the backscattered energy of the projectile). All the spectra are for a carbon projectile, except for Figure 1d, where a lithium projectile is used. The carbon-projectile-generated spectra show the lighter elements at the extreme left-hand side of the figure, with the broad peak on the right-hand side corresponding to the gadolinium film. The surface layer on the gadolinium is not resolved in these spectra. The gradual rise at low energy corresponds to backscattering from aluminum in the substrate (shown as A (sub) in Figure 1). The width of the broad peak allows the thickness of the gadolinium layer to be determined,[14] giving values of 2970, 2380, and 3570 Å for the aluminum, titanium, and mixed aluminum/silicon outer film samples, respectively. The lithium projectile allows the detection of the aluminum overlayer (shown as A (over) in Figure 1), which corresponds to the small sharp peak in the center of the spectrum.

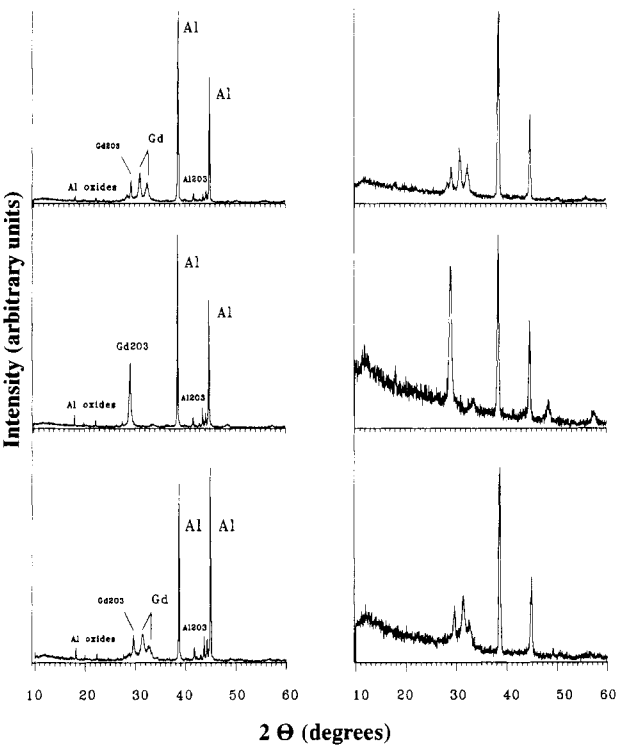

Figure 2. X-ray diffraction patterns of the films: (a) aluminum laser annealed outer film; (b) titanium laser annealed outer film; (c) aluminum/silicon coevaporated outer film. The pattern on the right is for the more surface-sensitive diffraction experiment.

The X-ray diffraction results for the three thin films are shown in Figure 2. The more bulk-sensitive diffraction pattern is on the left, and the more surface-sensitive pattern on the right. The spectra show features corresponding to the aluminum metal of the substrate. Additional peaks due to aluminum oxide on the substrate aluminum can be seen on the bulk-sensitive data. Peaks due to gadolinium metal and oxide are also identified, and the gadolinium metal and oxide region is shown expanded in Figure 3. As expected, the relative intensity of the substrate aluminum peaks to the gadolinium peaks is less for the surface-sensitive case. The details for the gadolinium region shown in Figure 3 are much the same for the surface- and bulk-sensitive regions. In the case of the two films that contained aluminum in the outer layer, Figure 3 shows a significant amount of Gd_2O_3, and perhaps $GdAlO_3$ and other $Gd_xAl_yO_z$ oxides, in addition to gadolinium metal. In the film with a titanium-laser-annealed

(11) Annual Book of ASTM Standards, Vol 03.06 published in *Surf. Interface Anal* **1988**, *11*, 112.
(12) Sherwood, P. M. A. *Practical Surface Analysis by Auger and Photoelectron Spectroscopy*; Briggs, D., Seah, M. P., Eds.; Wiley: London, 1983; Appendix 3.
(13) Ansell, R. O.; Dickinson, T.; Povey, A. F.; Sherwood, P. M. A. *J. Electroanal. Chem.* **1979**, *98*, 79.
(14) Northcliffe, L. C.; Schilling, R. F. *Nucl. Data* **1970**, *A7*, 233.

Table I. Binding Energies for the Silicon/Aluminum Film

		binding energy, eV				
sample	region	silica	Al–silicate	hydroxide	oxide	element/metal
before etch	Si 2p	103.3 (60%)	102.1 (27%)			99.5 (13%)
	O 1s			530.6		
	Al 2p		74.5			
etch 3 min	Si 2p		102.1 (78%)			99.5 (22%)
	C 1s			530.6 (85%)	529.5 (15%)	
	Al 2p		74.5			
etch 6 min	Si 2p		102.1 (69%)			99.5 (31%)
	O 1s			530.9 (48%)	529.6 (52%)	
	Al 2p		74.5			
etch 16 min	Si 2p		101.7 (57%)			99.5 (43%)
	O 1s			530.7 (63%)	529.2 (37%)	
	Al 2p		74.5			
etch 31 min	Si 2p		102.0 (45%)			99.6 (55%)
	O 1s			531.9 (49%)	529.6 (51%)	
	Al 2p		74.8 (93%)			72.1 (7%)
etch 41 min	Si 2p		102.0 (38%)			99.7 (62%)
	O 1s			531.9 (40%)	529.6 (60%)	
	Al 2p		74.8 (89%)			72.1 (11%)
etch 61 min	Si 2p					99.5
	O 1s			532.2 (28%)	529.7 (72%)	

outer layer, the gadolinium layer appears completely oxidized.

No significant difference was found in the films in Rutherford backscattering and XRD spectra before and after laser annealing, though the relative intensities of the aluminum substrate to gadolinium peaks in the XRD studies indicated some loss of outer film material resulting from the laser annealing process.

X-ray photoelectron spectroscopic studies of the films were carried out to monitor the surface layer and to profile through the layer by using argon-ion etching. The aluminum and silicon/aluminum outer layer films were depth profiled by using argon-ion etching. The titanium outer layer film was studied by angle-resolved photoemission and after heating over a range of temperatures.

Titanium-Laser-Annealed Surface Film. Heating Studies. The film with a laser-annealed surface film was studied over a range of temperatures. Titanium has a range of oxidation states, and elevated temperatures can cause a reduction of higher oxides to lower oxides. The normal oxide film on titanium is the stable TiO_2 oxide. Studies at ambient temperature show that the oxide layer after laser annealing is TiO_2 with no lower oxides. The surface layer shows two O 1s peaks corresponding to oxide (530.0 eV) and hydroxide (532.5 eV), with the latter increasing from 40% to 55% on going to increasingly surface-sensitive angle (80° to 30°), indicating a higher surface concentration of hydroxide. Figure 4 shows the Ti 2p region over a range of temperatures at normal takeoff angles. At ambient temperatures the Ti 2p region shows TiO_2 (Figure 4 shows mainly the Ti $2p_{3/2}$ region with a clear peak at 458.2 eV), but as the temperature is increased the TiO_2 decomposes with the formation of a long tail toward lower binding energy, corresponding to the formation of titanium metal and lower titanium oxides (see ref 15 and references therein). At 400 °C the spectrum (Figure 4c) shows two peaks corresponding to the Ti 2p spin-orbit doublets (Ti $2p_{1/2}$ = 459.6 eV, Ti $2p_{3/2}$ = 453.5 eV) of titanium metal. The spectrum stays much the same after the sample is cooled to ambient temperatures. There is little change in the O 1s spectral region during these temperature changes.

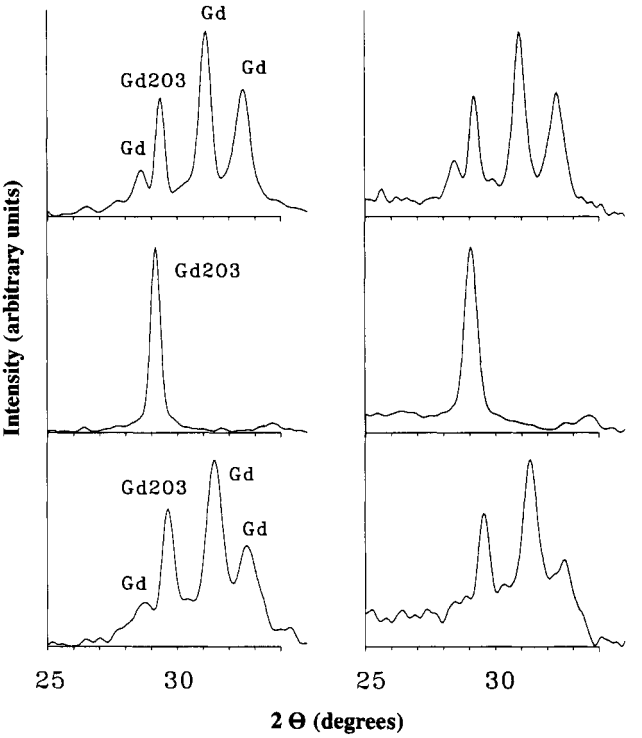

Figure 3. Gadolinium region of the X-ray diffraction patterns of the films. Parts a–c are for the same sample as in Figure 2. The pattern on the right is for the more surface-sensitive diffraction experiment.

We thus conclude that laser annealing does not change the nature of the oxide layer on the titanium film, which retains its very stable TiO_2 oxide layer.

Silicon/Aluminum Coevaporated Film. Depth Profile Studies. The silicon/aluminum coevaporated film showed significant changes in the O 1s, Si 2p, and Al 2p regions while the film was profiled by argon-ion etching. Figure 5 shows the overall depth profile which indicates the concentration changes in the outer silicon/aluminum film with depth, and Table I lists the binding energies. The concentrations shown in Figure 5 give only an approximate guide to concentration, since the concentrations are calculated by assuming that the components are in a homogeneous layer, rather than the actual, possibly complex, layer. Since the thickness of this outer film is about 200 Å and the outer film is removed in about 30–50 min,

(15) Hoflund, G. B.; Yin, H.-L.; Grogan, A. L., Jr.; Asbury, D. A.; Yoneyama, H.; Ideka, O.; Tamura, H. *Langmuir* **1988**, *4*, 346. Carley, A. F.; Chalker, P. R.; Riviere, J. C.; Roberts, M. W. *J. Chem. Soc., Faraday Trans. 1*, **1987**, *83*, 351.

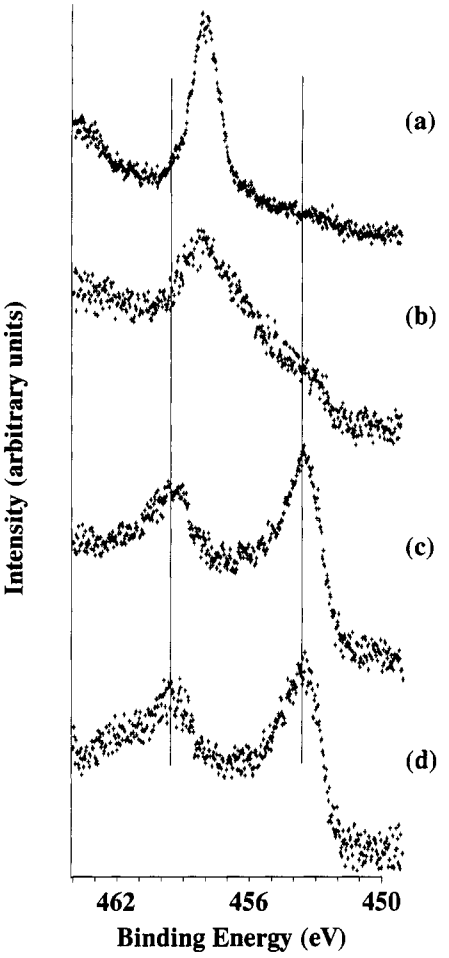

Figure 4. Ti 2p XPS spectrum of Al/Gd/Ti laser annealed alloy recorded at different temperatures: (a) ambient; (b) 200 °C; (c) 400 °C; (d) ambient after heating to 400 °C. The vertical lines show the Ti $2p_{1/2}$ and Ti $2p_{3/2}$ peaks of titanium metal.

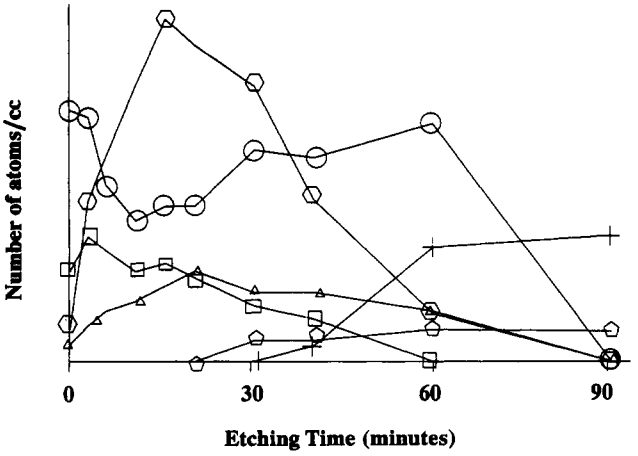

Figure 5. Depth profile of Al/Gd/Si–Al alloy showing how the relative number of atoms/cm^3 for each component varies with argon-ion etching time: O, oxygen; □, silicon (oxidized); △, silicon (elemental); +, gadolinium (metal and oxide); ○, aluminum (oxidized); ⬠, aluminum (metal).

the etch rate is about 4–7 Å-min. The outer layer–inner layer (gadolinium) interface is fairly broad but, as will be seen later, sharper than the interface for the laser-annealed sample.

The O 1s region shows a steady reduction in the hydroxide component (at higher binding energy) compared with the oxide component (from 85% to 28% after 61 min of etching). Some oxidation may have occurred during

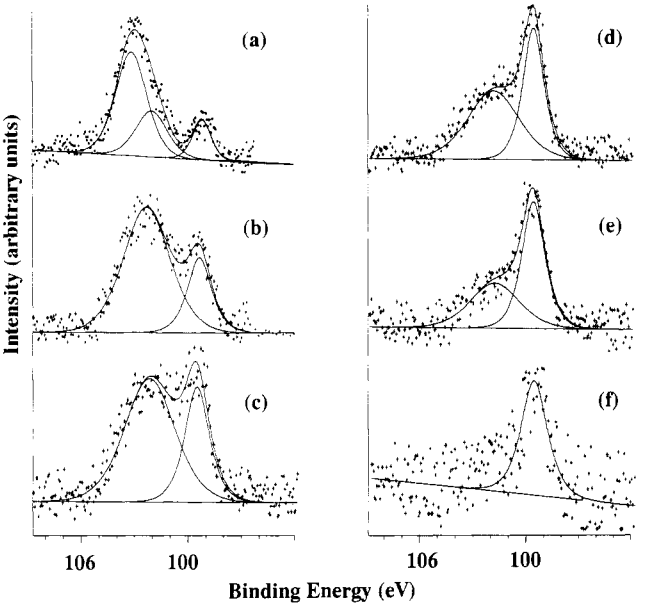

Figure 6. Si 2p XPS spectrum of Al/Gd/Si–Al alloy recorded at ambient temperature after increasing periods of argon ion etching: (a) before etching; (b) after 3 min of etching; (c) after 6 min of etching; (d) after 16 min of etching; (e) after 31 min of etching; (f) after 41 min of etching.

transfer (see above), though significant oxidation would have occurred in the film deposition environment. The Al 2p region shows a broad oxide peak at 74.8 eV that is probably a form of Al_2O_3. Calculation of possible shifts in aluminum oxides[16] suggest only a small (1.3 eV) range of binding energies for aluminum oxides and oxyhydroxides, so it is not possible to identify the specific oxide from the binding energy. The peak at 74.8 eV is believed to correspond to an aluminosilicate (for example, sillimanite,[17] Al_2SiO_5, has an Al 2p binding energy at about this value). Traces of aluminum metal are found after a very long etch period.

The Si 2p region (Figure 6) shows two peaks, the one at higher binding energy corresponding to oxidized silicon, and the one at lower binding energy corresponding to elemental silicon. Before etching is carried out, the oxidized silicon peak can be fitted to two components, the higher binding energy component (shifted by about 3.8 eV from the elemental silicon) corresponding to a form of SiO_2 and the lower binding energy component (shifted by about 2.6 eV from the elemental silicon) corresponding to silicon in aluminosilicate (in agreement with previous studies[17] of aluminosilicates). After only a short amount of etching (3 min) there is a considerable rise in the amount of aluminum (Figure 5) and the SiO_2 Si 2p peak is lost, leaving only aluminosilicate and elemental silicon Si 2p peaks. The amount of elemental silicon increases steadily with etching time.

Aluminum Laser Annealed Surface Film. Depth Profile Studies. The aluminum laser annealed film was first subjected to an initial 3-min etch and then exposed to air. The Al 2p spectra (Figure 7) showed a metal and oxide peak before etching, with a rather thinner oxide layer (around 25 Å based upon the relative intensities of the oxide and metal regions) than that found on air-exposed high-purity aluminum (about 30 Å). After an initial 3-min etch the relative amount of metal increased (Figure 7b), but after exposure to air and after a further 6-min etch no

(16) Wilson, G. R.; Sherwood, P. M. A., to be submitted.
(17) Wagner, C. D.; Passoja, D. E.; Hillery, H. F.; Kinisky, T. G.; Six, H. A.; Jansen, W. T.; Taylor, J. A. *J. Vac. Sci. Technol.* **1982**, *21*, 933.

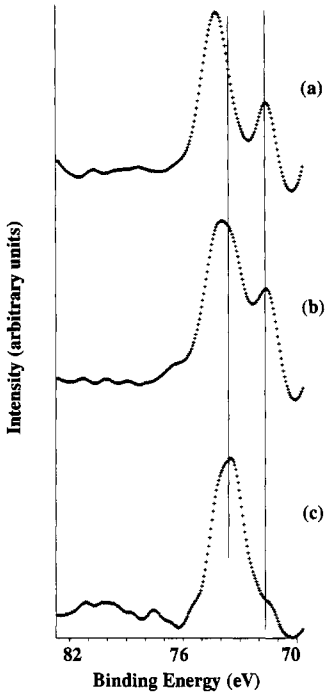

Figure 7. Al 2p XPS spectrum of Al/Gd/Al laser annealed alloy recorded at ambient temperature after increasing periods of argon-ion etching: (a) before any etching; (b) after an initial 3-min etch period; (c) after exposure to air followed by a 6-min etching period. The spectra were smoothed with a 23-point quartic/quintic smooth repeated 20 times. The vertical line at lower binding energy corresponds to aluminum metal (possibly an alloy), and the line at higher binding energy shows the oxide peak in spectrum c. There is a clear shift in oxide peak position.

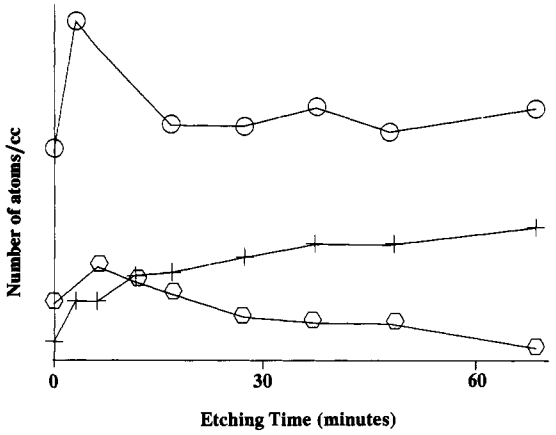

Figure 8. Depth profile of Al/Gd/Al laser annealed alloy showing how the relative number of atoms/cm^3 for each component varies with argon ion etching time: O, oxygen; O, aluminum oxide; +, gadolinium (metal and oxide).

metal can be seen. We thus conclude that the laser annealing has caused the aluminum to oxidize throughout most of the film. Some shift is seen in the oxide to metal separation in Figure 7, a feature that we have seen in other thin oxide films on aluminum.[18] Figure 8 shows the depth profile of the film after the initial 3-min etch and air exposure. The profile shows a slow reduction in the amount of aluminum and a slow increase in the amount of gadolinium. This broad interface between the outer layer and the inner gadolinium layer—broader (as measured from the slopes at the interface) than in Figure 5 (for a sample that was not laser annealed)—together with absence of metallic aluminum except near the surface suggests that the laser annealing has caused substantial mixing and oxidation of the outer aluminum layer. Evaporated aluminum layers without laser annealing give an Al 2p spectrum similar to that shown in Figure 7a, with steadily increasing amounts of aluminum metal as the film is profiled.

(18) Wilson, G. R.; Sherwood, P. M. A., to be submitted.

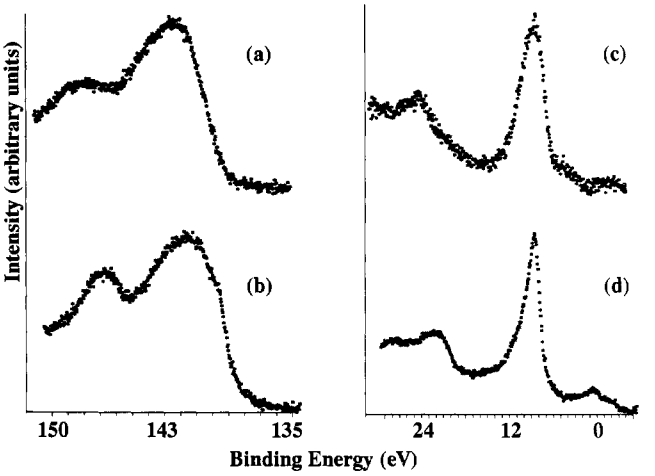

Figure 9. Gd 4d and valence band spectrum of gadolinium metal before and after argon-ion etching to remove the air-formed oxide film: Gd 4d region before (a) and after (b) argon-ion etching; valence band region before (c) and after (d) argon-ion etching. The most intense peak in the valence band region is due to Gd 4f electrons; the peak around 24 eV is due to Gd 5p electrons.

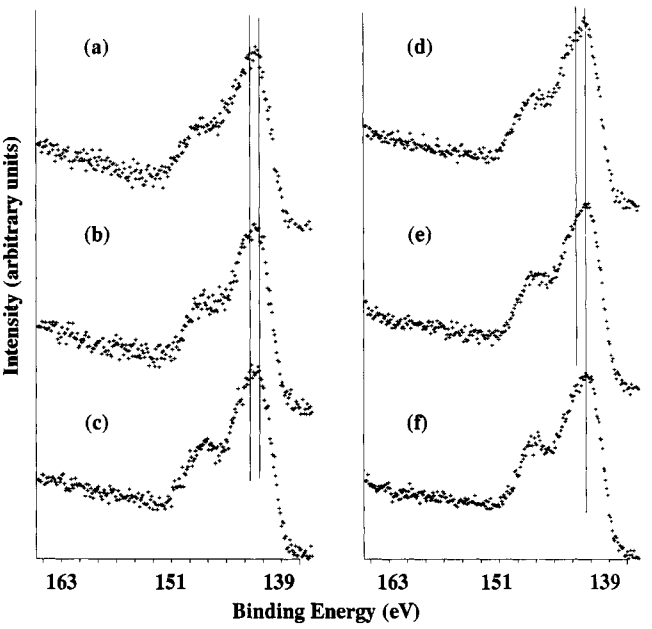

Figure 10. Gd 4d XPS spectrum of Al/Gd/Al laser annealed alloy recorded at ambient temperature after increasing periods of argon-ion etching: (a) after 3 min of etching; (b) after 6 min of etching; (c) after 11 min of etching; (d) after 16 min of etching; (e) after 26 min of etching; (f) after 36 min of etching. The vertical line at lower binding energy corresponds to metal, and the vertical line at higher binding energy corresponds to oxide. Spectra after 46 and 66 min of etching are identical with the metal spectrum observed in (f). Note how the oxide shoulder appears in spectrum e and grows in spectra e–a. Spectra a–c suggest that gadolinium is largely in the form of oxide.

The O 1s region shows a steady loss of hydroxide as the film is profiled. Gadolinium XPS data are provided by the Gd 4d and the valence band region. Figure 9 show these two regions for high-purity gadolinium before and after removal of the surface oxide layer. Surface studies of gadolinium have been fully discussed before,[19,20] and so

little will be said here. The Gd 4d region is very sensitive to oxidation: note that while the spectrum is broad, oxidation causes a rapid loss in the valley between the two peaks, together with a shift to higher binding energy. Significant changes are seen in the valence band of the pure metal on oxidation, but we do not report the valence band for the films because it will be a complex overlap of the valence band of the component metals and oxides. We recorded the Gd 4d region for all three films but will discuss the data for the aluminum film only. In the silicon/aluminum film the Gd 4d film is complicated by overlap from the Si 2s region, and for the titanium film (which was not depth profiled) little gadolinium intensity was seen. Figure 10 shows how the Gd 4d region changes for the aluminum laser annealed outer layer sample. The two vertical lines indicate the position of metal and oxide peaks. It can be seen that the amount of metal steadily increases with depth profiled. This is indicated by both the increasing amount of the metal component and the increasing valley between the two peaks.

Conclusions

Gadolinium films can be successfully coated with potentially protective films. Laser annealing can alter these protective films and in particular can mix these films with gadolinium to form a gently graded interface. Titanium-protective films appear to lose oxygen to the gadolinium, leading to substantial gadolinium oxidation. It is interesting to note that preferential oxidation of gadolinium has been found in GdFe and GdCo alloy thin films.[21] Aluminum and aluminum/silicon films appear to provide some protection for the gadolinium from oxidation, though some oxidation is found in the X-ray diffraction studies. The nature of the outer oxide layer in the aluminum/silicon evaporated films suggests the formation of aluminosilicates. In the aluminum laser annealed films there is very little metallic aluminum. In both aluminum-containing films the high oxidation of the outer layer seems to correspond to less oxidation and so more protection of the gadolinium inner layer. Some alloying between gadolinium and aluminum is also possible, but we have no direct evidence for alloy formation.

Acknowledgment. We are grateful to the Department of Defense for providing funding for the X-ray diffraction equipment and to Professor Basil Curnutte for assistance with the RBS measurements.

Registry No. Gd, 7440-54-2; Si, 7440-21-3; Al, 7429-90-5; Ti, 7440-32-6.

(19) Wandelt, K.; Brundle, C. R. *Surf. Sci.* **1985**, *157*, 162.
(20) Weller, D.; Sarma, D. D. *Surf. Sci.* **1986**, *171*, L425.
(21) Terzieff, P.; Lee, K. *J. Appl. Phys.* **1979**, *50*, 3565.

Fragment Formalism in Main-Group Solids: Applications to AlB_2, $CaAl_2Si_2$, $BaAl_4$, and Related Materials

Jeremy K. Burdett* and Gordon J. Miller*,†

Department of Chemistry and The James Franck Institute, The University of Chicago, Chicago, Illinois 60637

Received July 10, 1989

Some aspects of the structures of the anion nets in the $CaAl_2Si_2$ and $BaAl_4$ structure types are investigated by using the techniques of tight-binding theory. We examine the factors that stabilize main-group compounds that adopt AlB_2, $CaIn_2$, and $CaAl_2Si_2$ structure types for similar electron counts, i.e., the half-filled band. Traditional molecular orbital concepts and the method of moments are combined to compare the two structural isomers $CaAl_2Si_2$ and $BaAl_4$. Furthermore, we utilize two-dimensional pieces of these two structures as fundamental building blocks to form other main-group compounds.

In recent years the fragment formalism has been widely used to understand and even to predict the structures of inorganic and organometallic molecules, particularly in the area of metallocarboranes. (A recent book that uses this approach to look at a wide range of chemistry is listed in ref 1). The method relies on assembling the orbital picture for a complex system from its constituent fragments, whose structural and electronic characteristics are more easily understood, usually by analogy with simpler systems. To name only one example, the coordination preference for an olefin to an octahedrally based $Fe(CO)_4$ unit is readily clarified by using the frontier orbitals of the two fragments.[2] For extended solids, we have previously shown its utility for examining the electronic factors that control the structural properties of several main-group materials constructed from planar and puckered 6^3 sheets (two-dimensional tessellations of hexagons),[3] as well as the structures of PdXY (XY = P_2, PS, S_2).[4]

In this paper we apply these arguments to structures that contain two prevalent infinite two-dimensional networks:[5] (1) the trigonal $^2_\infty[Al_2Si_2]^{2-}$ bilayer found in $CaAl_2Si_2$;[6] (2) the tetragonal $^2_\infty$[PbO] layer of PbO.[7] Except

†Current address: Max Planck Institut für Festkörperforschung, Heisenbergstrasse 1, 7000 Stuttgart 80, West Germany.

(1) Albright, T. A.; Burdett, J. K.; Whangbo, M.-H. *Orbital Interactions in Chemistry*; Wiley: New York, 1985.
(2) Burdett, J. K. *Molecular Shapes*; Wiley: New York, 1980.
(3) Burdett, J. K. *J. Am. Chem. Soc.* **1980**, *102*, 450.
(4) Burdett, J. K.; Coddens, B. A. *Inorg. Chem.* **1988**, *27*, 418.
(5) Villars, P.; Calvert, L. D. *Pearson's Handbook of Crystallographic Data for Intermetallic Phases*; American Society for Metals: Metals Park, 1985.
(6) Gladyshevskii, E. I.; Kipyakevich, O. I.; Bodak, O. I. *Ukr. Fiz. Zh. (Russ. Ed.)* **1967**, *12*, 447.
(7) Wells, A. F. *Structural Inorganic Chemistry*, 5th ed.; Oxford University Press: London, 1984.

0897-4756/90/2802-0012$02.50/0